Development of an Advanced Clothing Model that Considers Heat and Moisture Transport

Mark A. Hepokoski[1], Timofey Golubev[2], Scott D. Peck[3]
ThermoAnalytics, Inc., Calumet, MI, 49913

Shailesh Gupta[4], Kevin Ward[5], Joel Coffel[6]
W.L. Gore & Associates, Inc., Elkton, MD, 21921

Michael K. Ewert[7]
NASA Johnson Space Center, Houston, TX, 77058

Despite recent advancements in the development of human thermal physiology models, clothing is often considered in only a rudimentary manner, that is, as a boundary condition at the skin characterized by its bulk thermal and evaporative impedances. While such an approach may be sufficient for thermoregulation modeling of humans operating in relatively low thermal burden scenarios, e.g., within an office environment, a clothing thermal model that does not explicitly consider the layer-to-layer transport of vapor can yield incorrect results, especially under conditions corresponding to high thermal stress or extreme environments. For example, vapor diffusing through layers of clothing can reach its dew point, in which case a phase change will occur that can fundamentally affect the transport of moisture and heat within the clothing ensemble. Specifically, the evaporation and condensation of moisture within the fabric layers can affect liquid content and temperature and, ultimately, affect thermo-physiological response and thermal comfort perception. Development of an advanced clothing model that considers heat and moisture transport within the fabric layers can improve the accuracy of human thermal predictions in scenarios where clothing-based condensation and evaporation occur. This paper describes how a general heat transfer software modeling tool was modified to consider the transport of vapor, the storage of liquid, and the thermal effects of phase change within a clothing ensemble. The advanced clothing moisture model was tested by comparing its predictions to measurements derived from sweating hot plate experiments and human physiological experiments. The model was able to reproduce the thermal and moisture results from tests performed under conditions in which condensation within the clothing layers was known to occur. This study demonstrates the importance of considering layer-to-layer vapor transport in clothing models and its impact on human thermal modeling predictions.

[1] Chief Scientist, Research & Development, mah@thermoanalytics.com.
[2] Research Scientist, Research & Development, tg@thermoanalytics.com.
[3] Senior Research Scientist (Emeritus), Research & Development, sdp@thermoanalytics.com.
[4] Research Scientist, Comfort and Durability CoP/Fabrics Division, and shgupta@wlgore.com.
[5] Research Scientist, Comfort and Durability CoP/Fabrics Division, and kward@wlgore.com.
[6] Research Scientist, Comfort and Durability CoP/Fabrics Division, and jcoffel@wlgore.com.
[7] Life Support and Thermal Systems Analyst, Crew & Thermal Systems Division, michael.k.ewert@nasa.gov

Nomenclature

A	=	cross-sectional area
$C^m_{conv_{ik}}$	=	moisture convection conductor between nodes *i* and boundary (fluid) node *k*
$C^m_{diff_{ij}}$	=	moisture diffusion conductor between internal nodes *i* and *j*
c_p	=	specific heat
D_v	=	mass diffusivity
f_a	=	fraction of fabric layer surface area filled by liquid
f_t	=	fraction of fabric layer thickness filled by liquid
h	=	convection heat transfer coefficient
$h_{i/j}$	=	specific enthalpy of the vapor in node *i* or *j* having the highest humidity ratio
h_{imp}	=	specific enthalpy of the imposed water
$h_{l,i}$	=	specific enthalpy of the liquid in node *i*
$h_{s,i}$	=	specific enthalpy of the solid in node *i*
K_M	=	mass transfer coefficient
k	=	conduction heat transfer coefficient
L	=	distance between communicating thermal nodes
$\dot{m}$	=	mass transfer rate
$\dot{m}_a$	=	mass flow rate of the air
m_i	=	mass of i^{th} control volume
$\dot{m}_{imp}$	=	imposed water flux
$\dot{Q}_{imp}$	=	imposed heat flux
$\dot{q}$	=	heat transfer rate
R	=	overall fabric layer thermal resistance
R_{dry}	=	dry fabric thermal resistance
R_{wet}	=	wet fabric thermal resistance
T	=	temperature
T_i	=	temperature of node *i*
T_f	=	fluid temperature (convection boundary condition)
V_i	=	total control volume associated with node *i*
$V_{l,i}$	=	volume occupied by the liquid in node *i*
ρ_a	=	air density
$\rho_{l,i}$	=	density of the liquid in node *i*
$\rho_{s,i}$	=	apparent density of the solid in node *i*
ϕ	=	liquid biasing factor defining directionality of liquid accumulation in a fabric layer
ω	=	humidity ratio
ω_i	=	humidity ratio of node *i*
ω_f	=	fluid humidity ratio (convection boundary condition)
ω_{sat}	=	saturated humidity ratio

I. Introduction

Human thermal modeling is used in Earth and space applications where it is cheaper and/or safer to determine thermal comfort and heat or cold tolerance limits by analysis than by testing. Various models have been used since the beginning of the space program to help design and test operational limits of space suits and emergency suits in extreme environments. Other models have been used to help establish design parameters for environmental control systems during high metabolic rate activities such as exercise or emergency egress. In these situations, sweating is likely to occur, which affects heat and mass transfer. Thus it is important to accurately model both heat and moisture movement between the person, their clothing, and their environment. However, despite recent advancements in the development of human thermal physiology models, clothing is often considered in only a rudimentary manner, that is, as a boundary condition at the skin characterized by its bulk thermal and evaporative impedances.[1-4]

Simple clothing models that only consider the latent heat of evaporation at the skin may be sufficient for thermoregulation modeling of humans operating in relatively low thermal burden scenarios, e.g., within an office environment; however, a clothing thermal model that does not explicitly consider the layer-to-layer transport of vapor

can yield incorrect results, especially under conditions corresponding to high thermal stress or extreme environments. For example, it is possible for vapor diffusing through layers of clothing to reach its dew point, in which case a phase change will occur that can fundamentally affect the transport of moisture and heat within the clothing ensemble. Specifically, the evaporation and condensation of moisture within the fabric layers can affect liquid content and temperature and, ultimately, affect thermo-physiological response and thermal comfort perception. Development of an advanced clothing model that considers heat and moisture transport within the fabric layers can improve the accuracy of human thermal predictions in scenarios where clothing-based condensation and evaporation occur.

II. Methods

A. Coupled Moisture and Heat Transport

A commercial heat transfer software tool (TAITherm®, ThermoAnalytics, Inc.)[5] was modified to consider the transport of vapor and the storage of vapor and liquid moisture within a clothing ensemble. TAITherm is a general thermal solver capable of modeling combined conduction, convection, radiation, and advection heat transport processes under transient or steady-state conditions. Solutions are obtained by finding temperatures that produce simultaneous energy balances on a network of thermal nodes. The nodal network is derived from a finite volume discretization of the geometry.

For portions of the domain having a moisture component, a moisture node is created coincident with the thermal node for that location. Just as a thermal node represents the temperature at a location, a moisture node represents the mass of moisture present at the location. The initial implementation considered the presence of both liquid and vapor, but only the transport of vapor, for which the metric is the humidity ratio, defined as the ratio of the mass of water vapor present to the mass of dry air present. With this metric, there are direct analogies between the conduction, convection, and advection modes of heat transport and mass transport (conduction of heat is equivalent to diffusion of mass). The analogies are shown in Table 1 and Figure 1. Mass transfer rate $\dot{m}$ is analogous to heat transfer rate $\dot{q}$, and humidity ratio ω is analogous to temperature T. The moisture conductors are analogous to the thermal conductors in the thermal problem. The conduction thermal conductor is defined by kA/L, where k is the conduction heat transfer coefficient, A is the cross-sectional area across which heat transfer is occurring, and L is the distance between the communicating thermal nodes. The conduction (diffusion) moisture conductor is defined as $C^m_{diff} = \rho_a D_v A/L$, where ρ_a is the air density, and D_v is the mass diffusivity. The m superscript indicates participation in the moisture transport problem. Alternatively, if an evaporative resistance across a fabric is known, a moisture conductor is the reciprocal of the resistance, modified by a scale factor to account for the driving potential being humidity ratio instead of vapor pressure. For convection, the thermal conductor is defined by hA, where h is the convection heat transfer coefficient, while convection moisture conductors are defined as $C^m_{conv} = K_M A$, where K_M is the mass transfer coefficient. For advection, the thermal conductor is given by $\dot{m}_a c_p$, where $\dot{m}_a$ is the mass flow rate of the air and c_p is the specific heat of the air. A value of unity takes the place of specific heat for the moisture transport advection conductor.

Table 1. Analogy between heat transport and moisture transport.

	Heat transport	Moisture transport
Conduction (diffusion)	$\dot{q} = -(kA/L)\nabla T$	$\dot{m} = -C^m_{diff}\nabla\omega$
Convection	$\dot{q} = hA(T - T_f)$	$\dot{m} = C^m_{conv}(\omega - \omega_f)$
Advection	$\dot{q} = \dot{m}_a c_p T$	$\dot{m} = \dot{m}_a \omega$

By considering conservation of mass and energy on each control volume, we can formulate a set of coupled moisture and heat transfer equations for each thermal-moisture node pair. Consider a control volume containing solid, liquid, and a water vapor/air mixture. The amount of solid material is fixed. The amount of water can change through evaporation, condensation, or exchange with an external source (imposed mass flow rate). For this model, no liquid is allowed to move across the control volume boundary. The amount of water vapor in the vapor/air mixture can change via mass transport across the control volume boundary, or by evaporation or condensation. Evaporation or condensation does not change the total amount of water (liquid plus vapor) within the control volume, nor does it subtract or add energy to the control volume. It does result in a change in the thermodynamic state within the control volume. The thermodynamic state is determined by the enthalpy and density of the control volume. It is assumed that all components within the control volume are at the same temperature.

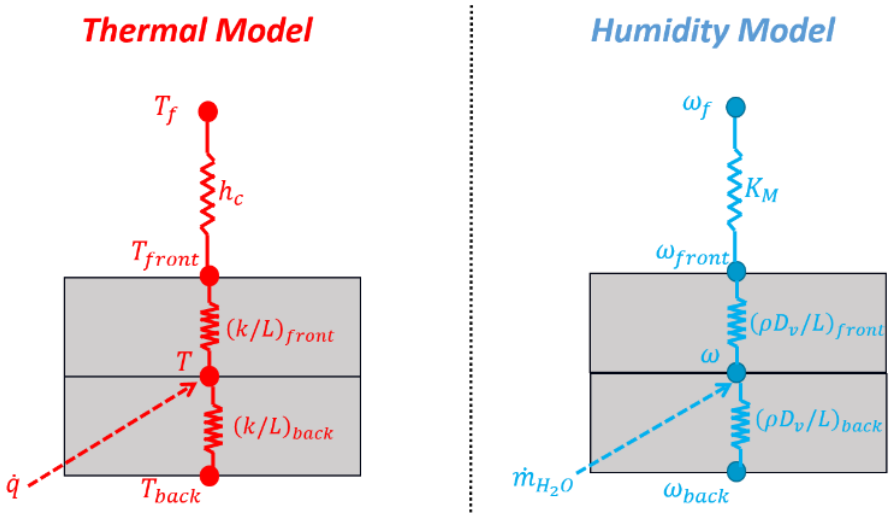

Figure 1. Heat and moisture transport analogy.

The mass of the i^{th}control volume is assumed to be the sum of the solid and liquid masses (the mass of air is two orders of magnitude smaller than both liquid water and typical clothing material masses and therefore neglected)

$$m_i = \rho_{s,i} V_i + \rho_{l,i} V_{l,i} \tag{1}$$

where V_i is the total control volume, $V_{l,i}$ is the volume occupied by liquid, $\rho_{s,i}$ is the apparent density of the porous solid material (i.e., the mass of material per unit external volume, including all of the pores in the material), and $\rho_{l,i}$ is the density of the liquid. The energy in the i^{th} control volume is measured by the product of the specific enthalpy (h) and the mass (m) of the solid and liquid mixture in the control volume, and can be expressed as

$$(mh)_i = \rho_{s,i} V_i h_{s,i} + \rho_{l,i} V_{l,i} h_{l,i} \tag{2}$$

where $h_{s,i}$ and $h_{l,i}$ are the specific enthalpies of the solid material and liquid, respectively, at the temperature of the control volume. Mass in the form of water vapor can cross the boundary of a control volume via diffusion or convective mass transfer, due to a vapor density differential. The transient mass balance for vapor entering or leaving a moisture node is expressed as

$$\sum_j C^m_{diff_{ij}} (\omega_j - \omega_i) + \sum_k C^m_{conv_{ik}} (\omega_k - \omega_i) + \dot{m}_{imp} = 0 \tag{3}$$

If both liquid and vapor are present simultaneously in the control volume, then the relative humidity is 100% and $\omega_i = \omega_{sat}(T_i)$ with the transient of liquid water volume being

$$\rho_l \frac{dV_{l,i}}{dt} = \sum_j C^m_{diff_{ij}} \left(\omega_j - \omega_{sat}(T_i)\right) + \sum_k C^m_{conv_{ik}} \left(\omega_k - \omega_{sat}(T_i)\right) + \dot{m}_{imp} \tag{4}$$

A transient energy balance of the control volume requires

$$\frac{d(mh)_i}{dt} = \sum_j C_{diff_{ij}} (T_j - T_i) + \sum_k C_{conv_{ik}} (T_k - T_i)) + \sum_j C^m_{diff_{ij}} (\omega_j - \omega_i) h_{i/j} + \sum_k C^m_{conv_{ik}} (\omega_k - \omega_i) h_{i/k} + \dot{m}_{imp} h_{imp} + \dot{Q}_{imp} \tag{5}$$

where $h_{i/j}$ is the specific enthalpy of the vapor in node i or j having the highest humidity ratio, h_{imp} is the specific enthalpy of the imposed water, and $\dot{Q}_{imp}$ is all other heat incident on node i, including radiation and imposed heat. The system of Equations 3-5 for each control volume are discretized in time using the Crank-Nicolson method, expressed in matrix form, and solved with the TAITherm matrix solver.

B. Application to Human Thermo-physiology Modeling

The above coupled heat and moisture transfer solver was combined with the TAITherm Human Thermal Model (HTM)[6] for modeling the effect of moisture on thermo-physiological response and thermal comfort perception. The HTM acts on a nodal network describing a human, adding unique properties and boundary conditions to create a complete thermophysiological description of the human body. Metabolic heating, shivering, respiration, sweating and peripheral vasomotion, etc. are the major physiological responses modeled to simulate a human body as it attempts to maintain homeostasis (Figure 2). These responses are used to adjust the coefficients of the bio-heat transfer equation[7], which is solved to predict skin and core temperature response to rapidly changing and asymmetric environments. The TAITherm HTM interacts with the simulated thermal environment and provides a suite of comfort metrics as output.

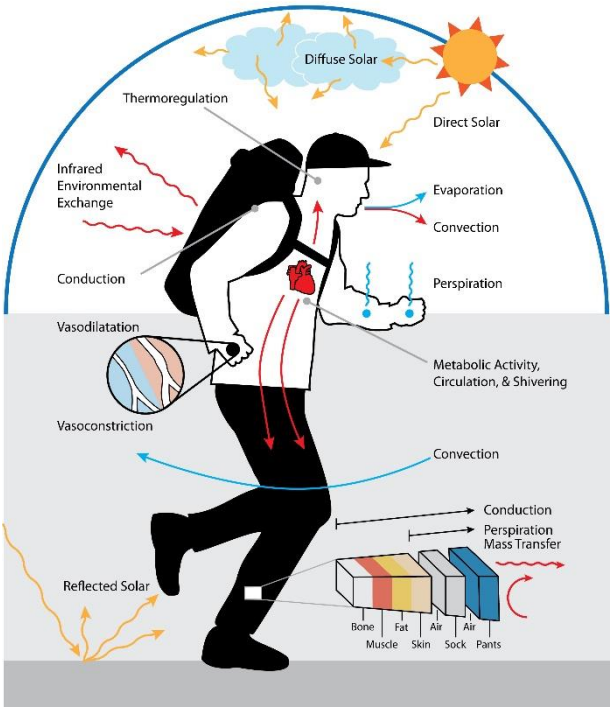

Figure 2. Thermo-physiological responses necessary to simulate a human body as it attempts to maintain homeostasis.

The geometric description of the human body within the HTM is described by a "shell element" mesh so that boundary conditions can be accurately applied and temperatures can be calculated across the skin surface and within the 16 tissue layers that are used to represent a human. The model computes temperatures at each element, from the surface of the clothing to the core of the body segment. Heat storage, three-dimensional conduction (between neighboring elements), and the heat transferred due to changes in blood flow, metabolism and sweating at the skin surface are all considered within the model. The shell elements can be grouped into physiological body segments that share the same thermal properties. These physiological body segments are subsequently subdivided into "body parts" where unique clothing properties can be applied. When manikin-derived clothing measurements are available, the body parts can be defined such that they match the zones of the manikin and map one-to-one to the corresponding body segment, allowing sub-segment clothing resistances to be applied.

A conceptual diagram of the HTM nodal network at an element with clothing layers added is shown in Figure 3. (Note that Figure 3 is a schematic representation and does not show all 16 tissue layers that are used by the TAITherm HTM to model a human body). Tissue temperatures at thermal nodes (●) are computed using the bio-heat equation.[7] Temperatures, humidity, and liquid content through clothing layers are computed using clothing evaporative and thermal resistance values specified from databases and the solution of the coupled moisture and heat transfer equations described above. The clothing layers and boundary conditions are modified with moisture nodes augmenting the thermal nodes (◔). Temperature and moisture gradients are computed within clothing layers both in the 'through the thickness' direction, and in the 'in-plane' direction, using clothing thermal and evaporative resistances (▬). Heat and mass transfer is computed between the outer clothing layer and the surrounding fluid, using heat and mass transfer coefficients (▬▬▬). The ambient temperature and relative humidity can be specified as a function of time in a weather file, or specified as a boundary condition. The resulting mass transfer rate at the skin layer is used to determine the evaporative cooling there.

The surface layers of the skin where evaporation occurs are modeled with two nodes. The interior skin node models the superficial cutaneous layer, where sweat glands are located and liquid moisture always present, hence the humidity ratio of this layer is set to its saturated value. The exterior skin node models the skin surface where sweat appears during active thermoregulation. The evaporative resistance between the two skin nodes defines the skin moisture permeability. The model uses an evaporative resistance of 0.3965 kPa·m^2/W, which was determined by fitting to achieve the expected 6% skin wettedness for a 50th percentile thermoneutral nude male.[4] The value is comparable to the model developed by Fiala et al., which used an evaporative resistance of 0.3333 kPa·m^2/W.[2] In addition, the amount of moisture (sweat) is tracked at the skin layer as a balance between the sweat rate computed within the Human

Thermal Model and the evaporation to the environment. The maximum liquid content on the skin is generally limited to 35 g/m^2, which is the known capacity of skin to hold liquid from literature[2]. Any sweat in excess of this amount is modeled as dripping off of the skin. If conditions are such that condensation or evaporation would occur within a clothing layer, this is computed automatically. Below the two surface skin nodes, only the thermal problem is solved.

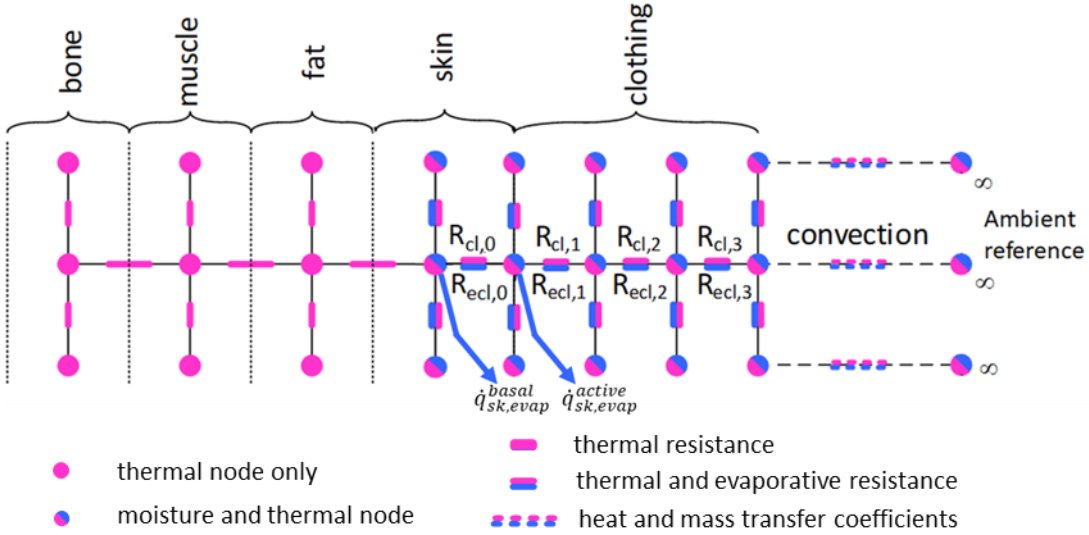

Figure 3. A schematic of the nodal network including tracking of vapor diffusion and liquid storage within a clothing ensemble.

The dependence of a fabric's vertical thermal resistance on liquid content is considered by interpolating between a measured dry thermal resistance (R_{dry}) and fully wet thermal resistance (R_{wet}) based on the amount of liquid accumulation relative to the material thickness. The directionality of liquid filling the layer is described by a liquid biasing factor ϕ with a value of zero representing a layer that is filled laterally, and a value of one representing a layer that is filled vertically. Values of ϕ in between zero and one represent a mixture of lateral and vertical filling and define the fractional layer filling as

$$\frac{f_a}{f_t} = \frac{\phi}{1-\phi} \tag{6}$$

where f_a is the fraction of the layer surface area filled by liquid and f_t is the fraction of the layer thickness filled by liquid. The overall layer thermal resistance is modeled as a parallel combination of two resistors, a "dry vertical" resistor, corresponding to portions of the surface area that are entirely dry, and a "mixed vertical" resistor, corresponding to portions of the surface area that have moisture (Figure 4).

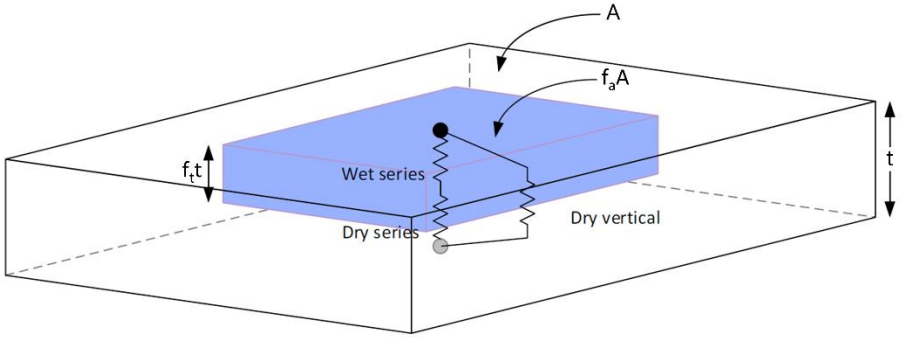

Figure 4. Modeling approach for dependence of a fabric's vertical thermal resistance on liquid content.

The dry vertical resistance is given by

$$R_{dv} = \frac{t}{k_{dry}A(1-f_a)} = \frac{1}{(1-f_a)}R_{dry} \tag{7}$$

where $R_{dry} = t/(k_{dry}A)$ is the thermal resistance (in m^2·K/W) of the fabric layer when it is completely dry. The mixed vertical resistor is a series combination of a wet and dry resistor with resistance given by

$$R_{mv} = \frac{f_t t}{k_{wet} A f_a} + \frac{(1-f_t)t}{k_{dry} A f_a} = \frac{f_t}{f_a} R_{wet} + \frac{(1-f_t)}{f_a} R_{dry} \quad (8)$$

where $R_{wet} = t/(k_{wet}A)$ is the thermal resistance (in m^2·K/W) of the fabric layer when it is completely saturated with moisture. The overall thermal resistance of the layer is the parallel combination of R_{dv} and R_{mv}

$$R = \left[\frac{1}{R_{mv}} + \frac{1}{R_{dv}}\right]^{-1} = \left[\frac{f_a}{f_t R_{wet} + (1-f_t) R_{dry}} + \frac{(1-f_a)}{R_{dry}}\right]^{-1} \quad (9)$$

III. Results and Discussion

A. Effects of evaporation and condensation on fabric temperatures

The advanced clothing moisture model was first verified by qualitatively comparing its predictions to measurements derived from sweating guarded hot plate experiments focused on the prediction of phase change and its effect on temperatures within a clothing stack. Sweating guarded hot plates are comprised of a porous metal plate attached to a conductive metal block fitted with heating elements and a water reservoir.[8] The hot plate "sweats" by transferring water from the reservoir through the porous metal plate. When the hot plate is covered by fabric samples, the amount of power required to maintain the plate at a given temperature can be related to the thermal and evaporative resistances of the materials.[9] Experiments were performed using a stack of three clothing materials (Figure 5a): a Gore-Tex® 3-layer laminate outer layer (GTX), a polyester lofted batting insulation middle layer (PEB), and a Capilene® (polyester fabric produced by Patagonia®) base layer (Cap). The thermal and evaporative resistance of each fabric in the stack was calculated from measurements using the ASTM F1868-17 standard[10] (Table 2, Method 1). The fabric layers were separated with films designed for moisture vapor transmission rate (MVTR) testing. These films allow the free passage of vapor, but prevent liquid transport to remove the effects of liquid diffusion between layers. Type-K thermocouples were sewn into both surfaces of each individual fabric (Figure 5b). Hot plate testing was executed under cool, humid ambient conditions (2 °C and 80% RH) in order to promote condensation within the layered stack-up when the hot plate's sweating feature was activated. Convection was controlled by imposing a 1.0 m/s wind speed.

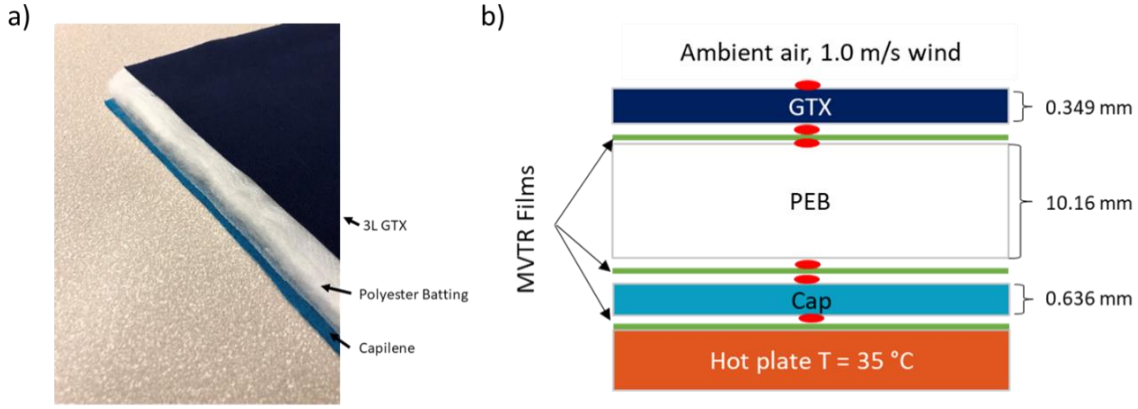

Figure 5. Wet and Dry Fabric Hot Plate. *a) Photograph of fabric stack showing the three clothing material layers. b) Diagram of fabric stack with thermocouple placement indicated by red ovals.*

Measurement of fabric temperatures was found to be challenging due to several experimental limitations. The addition of thermocouples for temperature measurement between the fabric layers introduces non-uniform air gaps, which add contact thermal resistance to the system. Additionally, each thermocouple is in contact with the fabric desired to be measured, as well as the MVTR film and the air gap. Therefore, the temperature measurements are not truly measuring the fabric temperature. We tried to control the size of the air gap between fabrics by adding hexagonal spacers (Figure 6a). While these spacers ensure a constant thickness air gap, they introduce a new problem of significantly non-uniform surface temperature distribution due to enhanced thermal conduction at the contact points of the spacers. The predicted effect of the spacers on local temperatures within each layer was found through

simulation to be up to 1.5 °C (Figure 6b, c). These non-uniform temperatures can affect the accuracy of the thermocouple measurements and introduce local areas of condensation and evaporation on a fabric surface. Therefore, we did not use the spacers in the tests where comparisons with models were made.

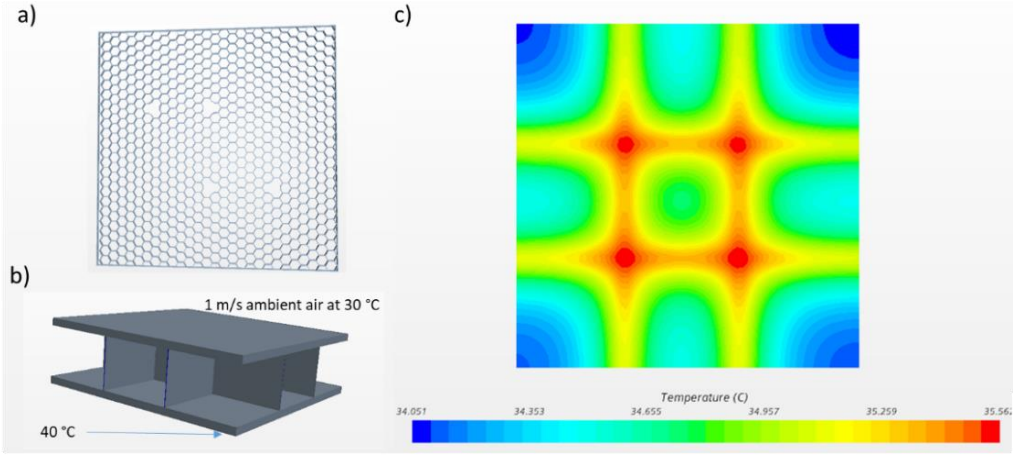

Figure 6. Air gap spacer geometry and simulation. *a) Air gap geometry. b) Simplified simulated geometry. c) Predicted temperature non-uniformities due to the spacer.*

Since no solution was found to overcome the non-uniform air gaps and inability to measure exactly a single fabric temperature, it was necessary to consider these uncertainties in the model. The main goal of this verification was to ensure that the clothing moisture model can correctly predict the locations of phase change in a fabric stack and their corresponding changes in temperature. Therefore, we first calibrated the model to match closely to the dry fabric temperature predictions by adding interstitial air layers and adjusting the individual thermal resistances of the fabric and air layers while maintaining the constraints that the total stack thermal and evaporative resistance must match the measured values. This adjustment takes into account the inaccuracy in thermocouple measurements due to simultaneous contact with several layers and non-uniform air gaps. The evaporative resistances were adjusted while preserving the measured ratio of thermal and evaporative resistance, which can be expressed as the product of the Lewis ratio (*LR*) and moisture permeability index (i_m) of each material[4]

$$i_m \cdot LR = R_{th}/R_e \tag{10}$$

The derived parameters for each layer using this method (Method 2) are shown in Table 2. This dry hot plate serves as a baseline for the wet (sweating) hot plate model, which is run without any further layer properties adjustments.

Table 2. Dry vs. Wet Hot Plate Test Case Fabric Properties. *Layer thicknesses and comparison of thermal and evaporative resistances of the layers in the fabric stack derived using two alternate approaches: the ASTM F1868-17 standard (Method 1) and our numerical fitting method (Method 2).*

Layer	**Thickness** *(mm)*	**Thermal Resistance** *(m^2·K/W)*		**Evaporative Resistance** *(m^2·Pa/W)*	
		Method 1	**Method 2**	**Method 1**	**Method 2**
GTX	0.349	0.006	0.012	11.44	22.98
Air/MVTR Film/Air	0.1*	N/A*	0.10	N/A*	6.061
PEB	10.16	0.185	0.05	24.43	6.612
Air/MVTR Film/Air	0.1*	N/A*	0.05	N/A*	3.03
Capilene	0.636	0.011	0.00515	4.28	1.997
Air	0.1*	N/A*	0.001	N/A*	0.3
MVTR Film	0.03	0.0008	0.0008	0.2	0.2
Air	0.1*	N/A*	0.01	N/A*	0.606
Stack Sum	**11.65**	**0.225**	**0.229**	**41.0±0.42**	**41.8**

*The thickness of the air gaps are non-uniform and therefore could not be accurately measured. The model uses an effective thickness which was determined through fitting the results to the measured dry hot plate temperatures.

The sweating hot plate was modeled by imposing the experimental boundary conditions and a liquid flux to the bottom side of the MVTR film that is in contact with the hot plate. The model was run until the temperatures reached steady state for comparison with experimentally measured temperatures. Measured and predicted fabric temperatures for the dry and wet hot plate tests are plotted in Figure 7. In the wet test, condensation occurs in the PEB and GTX layers, causing an increased fabric temperature due to the release of latent heat during the phase transition. Intuitively, one might expect to see condensation in all three layers, resulting in an increase in temperature. However, the Capilene layer experiences a decrease in temperature in the wet run. This is likely caused by the evaporation of liquid from the backside of the liquid barrier film that is in direct contact with the wet hot plate. The cooling of the liquid barrier film reduces the transmission of heat from the hot plate to the Capilene. We see good qualitative agreement between experimental and simulated results with the model correctly predicting the locations of evaporation and condensation. While experimental limitations in measuring reliable fabric temperatures as described above do not allow us to use this data for a rigorous validation of the moisture model, this set of tests verifies that the model is qualitatively accurate in prediction of phase change within a clothing stack. An experimental design that allowed for quantitative validation of the model is described in the next section.

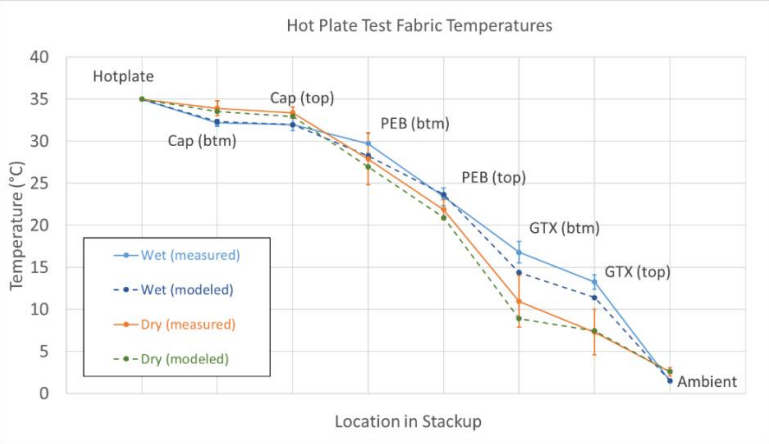

Figure 7. Wet and Dry Fabric Temperatures. *Top and bottom data point labels indicate the face closest to the hot plate ("btm") and the face closest to the ambient conditions ("top").*

B. Liquid Accumulation and Heat Flux

Given the multiple challenges with measuring accurate temperatures within the stack, we designed validation experiments that avoid the need for these measurements. These experiments focused on validating the model's ability to predict moisture content, transient heat flux, and the effects of liquid-dependent thermal resistance. Hot plate tests of a 3-layer clothing stack consisting of a fleece layer sandwiched between taffeta layers (Figure 8a) were executed under cool, humid ambient conditions (15 °C and 90% RH). The properties of the fabrics were measured independently and are provided in Table 3.

Table 3. Liquid Accumulation Validation Test Case Fabric Properties.

Layer	Thickness *(mm)*	Thermal Resistance *(m^2·K/W)*	Evaporative Resistance *(m^2·Pa/W)*
Air Boundary Layer	N/A	0.045	4.8
Taffeta	2	0.007	12.39
Fleece	5	Dry: 0.12, Wet: 0.03	11.54
Taffeta	1.5	0.007	12.39
Contact Resistance	1.5	0.0004	0.15

The fabric layers were separated with films that allow the free passage of vapor, but prevent liquid transport to remove the effects of liquid diffusion between layers. The hot plate tests were run for 18 hours in order to induce a significant liquid accumulation in the fleece which would cause a measurable transient in its thermal resistance. The measured weight gain due to liquid accumulation of each fabric layer was compared to the model's predictions. Additionally, the transient applied heat flux required to maintain a constant 40 °C hot plate temperature was measured and compared to the transient simulation. Condensation-induced liquid accumulation causes decreasing fabric thermal resistance, which results in an increasing heat loss over time. Therefore, the applied hot plate heat flux necessary to maintain a constant temperature increases with time.

The fabric stack was modeled in TAITherm. An imposed liquid flux was applied to the contact resistance layer to model the sweating hot plate. The liquid-dependent thermal resistance of the fleece layer was calculated according to Equations 6-9, using a liquid biasing factor of zero. The transient model's prediction of moisture accumulation in each layer (Figure 8b) and hot plate heat flux (Figure 8c) was within one standard deviation of the experimental results (average of three trials). The discrepancy between the shape of the measured and predicted curves could be due to the dependence of evaporation rate on the moisture accumulation within the fabric due to its internal structure, which is currently not considered in our model. More specifically, the S-shape of the measured curves could be due to the appearance of "free water" (water that is not strongly bound to the internal structure of the fabric) when the moisture content in the fleece increases causing a higher evaporation rate. Similar S-shaped curves have been obtained in the literature.[11] The sporadic larger error bars were due to the need to periodically replenish the hot plate water supply, which caused brief spikes in heat flux values. The larger error bars between 300 and 600 minutes into the experiments were due to the fact that the change in the slope of the curve occurred at slightly different time points in each of the three trials, which could be the result of slight differences in the initial conditions of the experiment, environmental conditions, and differences in air gaps when the stack was placed on the hot plate.

a)

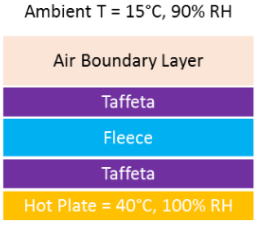

b)

Layer	Measured Weight Gain (g)	Predicted Weight Gain (g)
Taffeta	N/A	0
Fleece	140.5 ± 17.0	129.7
Taffeta	2.2 ± 0.4	2.3

c)

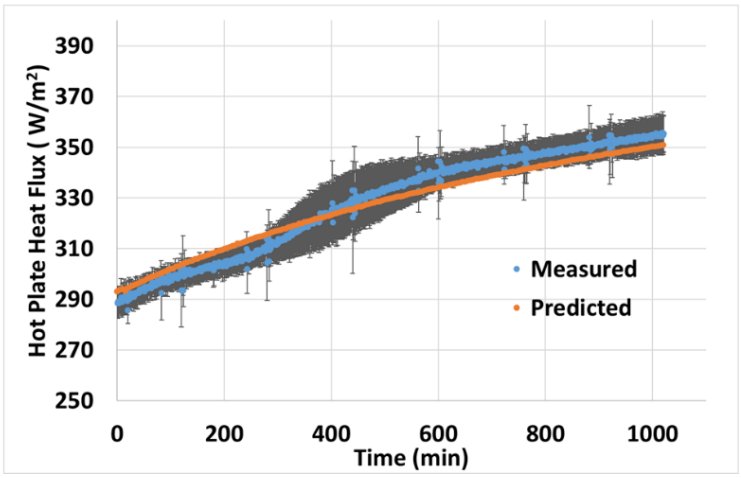

Figure 8. Model Validation. *a) Hot plate experiment clothing stack and boundary conditions, b) Layer weight gain due to liquid accumulation. c) Transient increase of hot plate heat flux due to liquid-dependent thermal resistance.*

C. Application to Human Modeling

The validated clothing moisture model was applied to model the thermo-physiological response of a clothed human undergoing a NASA work-rest cycle. This metabolic profile has been used to establish design parameters for the environmental control system of human spacecraft as found in the NASA Human Integration Design Handbook (Table 6.2-10).[12] The work-rest cycle consists of a 15 minute sedentary period, followed by a 30 minute period of vigorous exercise with a metabolic equivalent of task (MET) of 9 (1 MET = 58.2 W per 1 m^2 of body surface area), followed by a rest period. The cycle is performed in a room-temperature environment of 24 °C and 40% relative humidity. The human is modeled to be wearing a short-sleeve shirt (R_{th} = 0.11687 m^2·K/W, R_e = 0.0108 m^2·kPa/W) and shorts (R_{th} = 0.1 m^2·K/W, R_e = 0.012 m^2·kPa/W).

The results of two sweat evaporation models are compared: the first being the more simplistic model described in ASHRAE Fundamentals in which the basal and active thermoregulatory sweat evaporation rate is predicted in terms of a skin wettedness; and, the second being the advanced moisture modeling approach described in this paper in which the sweat evaporation is calculated by solving simultaneous heat and mass transfer equations for the skin surface and superficial cutaneous skin layer. There are 2 limitations in the ASHRAE model: 1) it is inherently not capable of considering storage of liquid sweat on the skin surface; and, 2) it assumes that the basal sweat evaporation (due to natural diffusion of vapor from the subcutaneous layer) is restricted to a constant wettedness corresponding to 6%. Figure 9 shows the skin and hypothalamus temperatures and the corresponding changes in sweat evaporation over the duration of the exposure. As expected, we see an increase in hypothalamus temperature during the exercise portion, followed by a decrease during the rest portion. Since the maximum liquid content of the ensemble was not measured, the effect of liquid storage is illustrated by running a simulation using an established value for a nude human (i.e., 35

g/m^2), which represents a lower bound, and a second simulation that allows for unlimited storage of liquid within the clothing, which represents an upper bound. We find that while the storage of liquid within the clothing may only have a small impact on core temperature, its impact on future evaporation rates and skin temperature may be significant. This numerical experiment serves as a simple test of the ability to couple the clothing moisture model with a human thermal physiology model (TAITherm Human Thermal Model) and predict qualitatively-accurate results.

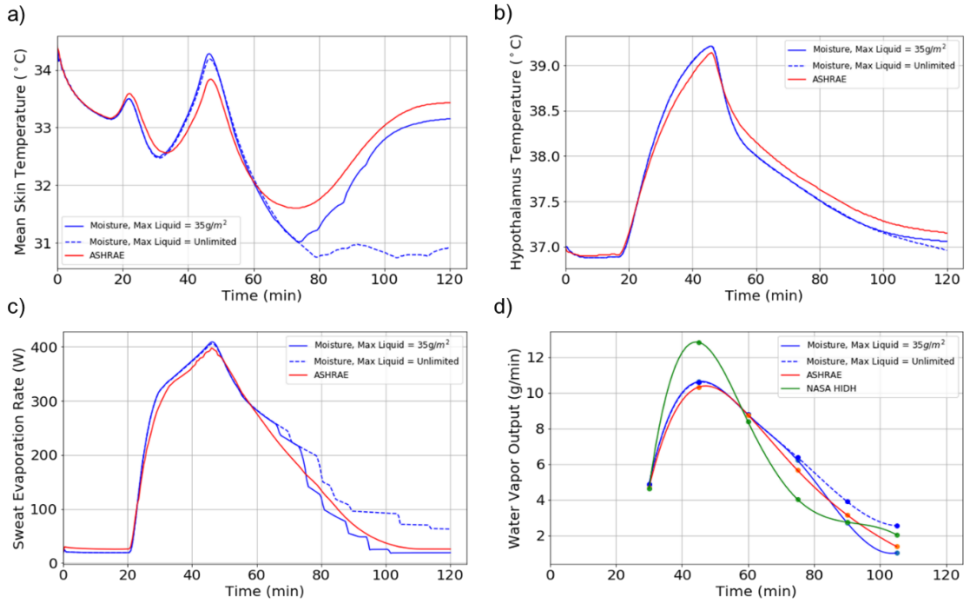

Figure 9. NASA Work-Rest cycle human thermal modeling results. *a, b, c) Comparisons of TAITherm simulation results for mean skin temperature (a), hypothalamus temperature (b) and sweat evaporation heat rate (c) from approaches that consider unlimited sweat accumulation, sweat accumulation limited to 35 g/m^2, and no tracking of sweat accumulation (ASHRAE approach) in the skin/clothing. d) Comparison of TAITherm computed water vapor output with results reported in the NASA Human Integration Design Handbook (HIDH).*

For an additional validation of human modeling with the moisture model, we compared the prediction of moisture accumulation in a clothing ensemble on a human under cold conditions to a study of protective textiles at low temperatures.[13] In this study, the subject trial was performed in a climatic chamber at -20 °C with the subject walking for 2 hours on a treadmill at 5.5 km/h. The clothing ensemble consisted of long john sports underwear, cotton briefs, fleece jacket, balaclava, gloves, tennis socks, cold protective socks, winter boots and an outer foul weather impermeable protective suit. The garment system had an overall thermal resistance of 350 x 10^{-3} m^2·K/W and evaporative resistance of 190 m^2·Pa/W. The study reported that the activity of the subject translates to a MET of 3.2, where 1 MET is the rate of energy produced per unit surface area of an average person seated at rest and defined as 58.2 W/m^2.[4] However, this metabolic rate needs to be adjusted to account for the extra work required to perform activity with heavy or restrictive clothing.[14] According to a British Standard (BS 7963:20007), the increase in MET due to wearing a highly insulated impermeable ensemble is 25-50 W/m^2.[15] This translates to an increase of approximately 0.4-0.9 MET. When using a MET rate of 3.9, the TAITherm model predicted moisture accumulation in the suit to be 121 g as compared to 90-130 g reported in the paper. This comparison confirms the validity of TAITherm-predicted moisture accumulation in human models.

IV. Conclusion

This study demonstrates the importance of considering layer-to-layer vapor transport in clothing models and its impact on human thermal modeling predictions. Validation of the advanced clothing moisture model described in this paper resulted in development of a methodology for deriving the properties of individual air and fabric layers within a stack, which may prove valuable for other researchers concerned with reconciling bulk thermal and evaporative resistances with their individual fabric layer components. Future work will involve further comparison of the model to human subject test data. The present study highlights the deficiencies of some sweat evaporation models (e.g.,

ASHRAE) for accurately predicting evaporation in scenarios wherein the liquid accumulation at the skin and clothing layers can be significant.

One limitation of the advanced clothing moisture model is that it does not consider fabric to fabric or in-plane wicking of liquid moisture, which is currently an area of active research. To overcome this deficiency, the sweating hot plate tests that were developed to validate the model were designed to mitigate transport of liquid moisture within the fabric stack. Despite the many difficulties encountered in developing and running the physical tests, the advanced clothing moisture model was able to reproduce the thermal and moisture behavior observed in the tests (often within one standard deviation of the measurements), which were performed under relatively extreme conditions where condensation within the clothing layers was known to occur.

It is hoped that the human thermal modeling improvements discussed here can be used to make more accurate predictions for both Earth and space applications. NASA uses may include predicting spacecraft heat and moisture loads during planned activities such as exercise or unplanned emergency situations that result in high activity levels. This could be useful for design and operational support of lunar Gateway and lunar surface missions as well as Mars missions of the future.

Acknowledgments

The authors would like to thank NASA for assistance and guidance on the preparation and presentation of this material as it concerns humans living in space and working in extreme environments. This material is based on research partially sponsored by ThermoAnalytics, Inc., W.L. Gore & Associates, the U.S. Army Natick Soldier Research, Development and Engineering Center (NSRDEC), and the National Aeronautics and Space Administration (NASA). The views and conclusions contained herein are those of the authors and should not be interpreted as necessarily representing the official policies or endorsements, either expressed or implied, of the U.S. Army Natick Soldier Research, Development and Engineering Center (NSRDEC), the National Aeronautics and Space Administration (NASA), or the U.S. Government.

References

[1]Hensley, D. W., Mark, A. E., Abella, J. R., Netscher, G. M., Wissler, E. H., and Diller, K. R., "50 Years of Computer Simulation of the Human Thermoregulatory System," *ASME. Journal of Biomechanical Engineering*, Vol. 135, No. 2, 2013.

[2]Fiala, D., Lomas, K.J., Stohrer, M., "A computer model of human thermoregulation for a wide range of environmental conditions: The passive system," *Journal of Applied Physiology*, Vol. 87, No. 5, 1999, pp. 1957-1972.

[3]Kobayashi, Y., Tanabe, S., "Development of JOS-2 human thermoregulation model with detailed vascular system," *Building and Environment*, Vol. 66, 2013, pp. 1–10.

[4]*2005 ASHRAE Handbook: Fundamentals*, American Society of Heating, Refrigeration and Air-Conditioning Engineers, Atlanta, 2005, pp. 8.1-8.29.

[5]TAITherm®, Software Package, Ver. 2020.1, ThermoAnalytics, Inc., Calumet, MI, 2020.

[6]TAITherm® Human Thermal Model (HTM), Software Package, Ver. 2020.1, ThermoAnalytics, Inc., Calumet, MI, 2020.

[7]Pennes H. H., "Analysis of tissue and arterial blood temperatures in the resting human forearm," *Journal of Applied Physiology*, Vol. 1, No. 2, 1948, pp. 93-122.

[8]ISO 11092:2014, "Textiles – Physiological effects – Measurement of thermal and water-vapour resistance under steady-state conditions (sweating guarded-hotplate test)," Retrieved from https://www.iso.org/standard/65962.html [cited 27 April 2021].

[9]Gibson, P. W., "Comparison of Sweating Guarded Hot Plate and Upright Cut Methods of Measuring Water Vapor Permeability," U.S. Army Natick Research, Development and Engineering Center, TR-92/046, Natick, MA, August 1992.

[10]ASTM F1868-17, "Standard Test Method for Thermal and Evaporative Resistance of Clothing Materials Using a Sweating Hot Plate," ASTM International, West Conshohocken, PA, 2017.

[11]Schneider, A.M., Hoschke, B.N., Goldsmid, H.J., "Heat transfer through moist fabrics," *Textile Research Journal*, Vol. 62, No. 2, 1992, pp. 61-66.

[12]"Human Integration Design Handbook (HIDH)," National Aeronautics and Space Administration, NASA/SP-2010-3407/REV1, Washington, DC, Approved: 06-05-2014.

[13]Bartels, V. T. and Umach, K. H., "Water Vapor Transport Through Protective Textiles and Low Temperatures," *Textile Research Journal*, Vol. 72, No. 10, 2002.

[14]Hepokoski, M., Gibbs, S., Curran, A., Coca, A., "Improving Adaptive Manikin PPE Testing with Virtual Simulation," *11th International Meeting on Thermal Manikin and Modelling*: Suzhou, China, 2016.

[15]Parsons, K.C., "Heat Stress Standard ISO 7243 and its Global Application," *Industrial Health*, Vol. 44, No. 3, 2006, pp. 368-379.